

PROGRESS REPORT ON THE CERN-PS LINAC

C.S. Taylor, D.J. Warner, F. Block and P. Têtu
European Organization for Nuclear Research
Geneva, Switzerland

Abstract

This paper discusses the behaviour of the CERN-PS Linac at currents of 50 to 100 mA. The difficulties of bunching at the higher currents are first described, and then the transverse beam properties at 50 - 60 mA, in particular blow-up, are discussed in detail as a background to the behaviour at 100 mA. The measures which are being taken to combat beam loading are described, and the heating effects of the high brilliance 500 keV beam mentioned. A method of emittance measurement using a computer is reported, and we give some comments on our experience with the statistical analysis of machine parameters.

Introduction

The duoplasmatron-short column combination (Refs. 1,2) was installed early this year during the PS shut-down which resulted from the motor-generator set failure. In early May, the 500 keV beam was injected into the linear accelerator and an accelerated beam of 100 mA was obtained within a few days, rising to 125 mA shortly after. Subsequently a stable beam of 135 mA was obtained. For normal injection into the PS the beam has been limited to 80 - 100 mA, corresponding to steady running around 10^{12} ppp in the PS, with a mean intensity of $1.028 \cdot 10^{12}$ averaged over a ten days' run, and a peak of $1.23 \cdot 10^{12}$.

The most noticeable immediate effect of the higher beam currents throughout the Linac as a whole was in the buncher, where one was troubled by an anomalous loading, and in the bunching factor, which dropped from 2.4 to 1.4. The beam loading in the tanks was, of course, more severe, but with partial compensation and debunching the energy spread was kept within reasonable limits. Another effect of the higher current was that it became more difficult to carry out and interpret beam measurements.

Bunching

Buncher Loading

An analysis of beam-loading in the CERN single-gap buncher shows that, following klystron theory, there should be resistive and reactive components of approximately $5 \text{ M}\Omega$ each across the $150 \text{ K}\Omega$ of the buncher shunt impedance at 500 mA beam current. The resistive component should produce a drop of 1.5% in the buncher voltage, assuming constant power input and neglecting stored energy. However, when the new

beam was first passed through the buncher, the voltage fell by 70% of its original value during the passage of the beam, with a time constant long by comparison with the $1.5 \mu\text{s}$ of the buncher cavity.

Since the buncher cavity is pumped only by the beam tube, and since the cavity is by no means a clean vacuum structure, it was suspected that bad vacuum conditions in the buncher gap contributed to the effect by encouraging inelastic processes. An attempt was made to reduce the total pressure by installing a small oil diffusion pump directly on the buncher cavity. This pump increased the estimated pumping speed in the cavity by 50%, but had no noticeable effect on the loading. However, as the weeks passed, the voltage drop was seen to diminish of its own accord, presumably by a "clean-up" process. Three weeks after the start, the voltage drop had fallen from 70% to 30%.

The buncher grids also came under suspicion as a possible source of low-energy electrons, both by thermal and secondary emission. One was led to the thermal emission possibility by the evidence of melting on stainless steel beam-limiting diaphragms. The grids were therefore removed about a month after the first tests and replaced by titanium diaphragms, having an aperture of 18 mm diameter. This change had very little effect.

Subsequently the loading phenomenon diminished still further, and by September the voltage drop was around 14%.

Although one would like to try to eliminate this effect altogether by improving the vacuum design, which means effectively building a new buncher, we do not wish to embark on this until the effect of space charge on the bunching process itself is better understood, since these considerations could lead to modified bunching schemes and hard-ware.

Space Charge and Bunching

As was mentioned in the Introduction, a salient feature of the machine at high currents is the low trapping efficiency and bunching factor. For example, during the first tests at 100 mA the ratio of accelerated to injected current was around 35%, and this figure has not been improved with time. In fact, at the present moment the efficiency is more nearly 30%, with a bunching factor of 1.4. Previously, one could obtain efficiency of 50% at 50 mA and 64% at 10 mA, with bunching factors of 2 to 2.5.

For an explanation of this inefficient trapping one looks naturally to space charge effects, both transverse and longitudinal. However, it is not easy to establish experimentally to what extent this inefficient trapping is caused by

- a) space charge limitation in the first few gaps of the accelerator, and/or
- b) space charge limitation in the buncher and drift space.

The evidence which we have at the moment is that even with the buncher voltage falling by 70% during the beam pulse, the output pulse was sensibly flat after an initially ragged front edge, i.e. the bunching factor was invariant over a wide range of buncher voltage. Another demonstration of this insensitivity to bunching voltage was obtained by measuring output current at a fixed time in the pulse versus buncher voltage (Fig. 1).

This result might suggest that a space charge limit is being approached in the accelerator itself, i.e. a point at which added charge spills out again, particularly as we have already passed the limit predicted by Bondarev and Vlasov (Ref. 3). Nevertheless we are concentrating on the alternative possibility - that the single-gap buncher sets the present limit to the proton current which can be injected into the Linac acceptance hypervolume, and that the limit is little dependent on bunching voltage. Several factors have influenced this approach:

- a) The buncher system applies a single longitudinal constraint to the proton beam which then travels 0.78 m (in 77 ns) via a single focusing triplet to the accelerating cavity. One expects the above system to be more vulnerable to space charge limitation than the accelerator proper with its longitudinal impulses applied every 5 ns and a complete focusing period every 20 ns.
- b) Major changes would be required to raise the space charge limit of the accelerator (e.g. $N = 1$ focusing system, higher injection energy, higher stable phase angle) whereas improvements in the bunching system might be comparatively straightforward.
- c) An adequate numerical treatment of bunching dynamics with space charge may be possible (and would be a valuable preliminary step towards more rigorous Linac dynamics computations) using experimental data from the transverse planes in the calculations.

Let us consider the last point in more detail. One expects that when space charge effects become serious they will oppose the velocity modulation introduced into the beam so that either it will be impossible to bunch the protons effectively or if the bunching is satisfactory longitudinally then the beam will have expanded transversely. A considerable amount of work seems to have been done on bunchers with space

charge when applied to electron beams in klystrons and travelling-wave tubes (Ref. 4). However, the usual conditions applicable to electron beams, e.g. small emittance, motion under Brillouin flow and approximately constant current density, are far from the usual proton beam conditions. It seems that for the CERN Linac there is little alternative to a numerical computation procedure which integrates step-by-step from buncher to Linac the equations of motion and electromagnetic fields appropriate to the initial conditions in the proton beam.

Some Observations on the Transverse Effects of Bunching

One can measure the transverse effects of the bunching process by the two slit method (see Automatic Emittance Measurements). Some of the effects thus revealed and discussed here are not specifically related to high intensity but are useful in that we meet in the bunching region the problems of the accelerating gaps in essence. In addition, the difficulties one finds in interpreting results and justifying experimental methods are typical of the complications introduced by the high current phenomena in all Linac experiments.

A first indication of a transverse effect was that the current injected into the first half drift tube of the Linac decreased when the buncher (both with and without grids) was energized. Later, the emittance and density distributions at the half drift tube were measured with the buncher (no grids) off and on, for both maximum and reduced currents, with constant emittance at the buncher input. The triplet focusing, buncher and accelerator conditions were set for optimum beam acceleration conditions before performing the measurements. The results may be summarized as follows:

A. Effect of Powering the Buncher for Injected Current, 100 mA

- i) A slight rotation effect corresponding to a defocusing lens at the buncher of strength $< 0.2 \text{ m}^{-1}$;
- ii) a constant current of 100 mA at the first half drift tube;
- iii) a decrease in phase space density in the centre of the phase plane to $\sim 90\%$ of the unbunched density;
- iv) an increase in normalized area from 0.29 to $0.35 \text{ } \mu\text{cm mrad}$.

B. Effect of Powering the Buncher for Injected Current, 350 mA

- i) A rotation of the emittance figure, corresponding to a (defocusing) lens at the buncher of strength $\sim 1.2 \text{ m}^{-1}$;
- ii) a reduction of the current at the first half drift tube from 350 mA to 260 mA;

- iii) a decrease in phase space density, mainly at the centre of the plane and typically to ~64% of the unbunched density;
- iv) a slight emittance change, which is not meaningful as the normalized emittance area of 0.75π cm mrad is that dictated by the aperture of the triplet lens.

It can be shown that for 17 keV axial energy modulation by the buncher, the transverse effect is of a lens oscillating at 200 Mc/s between strengths $\pm 1.0 \text{ m}^{-1}$ with the protons accepted by the Linac corresponding mainly to the maximum defocusing lens. The measured emittance blow-up in the non-aperture-limited case (Experiment A) presumably corresponds to the integrated envelope of the oscillating emittance; in the aperture-limited case at higher current (Experiment B) the triplet is set to match the maximum defocusing part of the oscillating emittance to the Linac acceptance and reject the rest, resulting in a large current loss, a measured rotation of the predicted order, and a decrease in density (see remarks on the hypervolume later), due partly to space charge effects.

Let us now discuss the uncertainties in comparing low and high current results.

The slit methods of emittance measurement are not rigorous at high current densities as

- a) one still assumes straight line trajectories, and
- b) one assumes that suppression of most of the beam at the first slit does not alter the subsequent motion of the other protons.

Effect b) is especially important in explaining result B.iii) because the first slit is only 25 cm from the buncher gap and the longitudinal space charge effects really act on the selected beam strip as it travels between the slits. However, the sum of the measured current elements was only 10% higher than the measured total for 350 mA and 5% higher for 100 mA. Note that the 100 mA beam is obtained by "sieving" the 350 mA beam so both beams start with the same effective emittance. The higher effective emittance subsequently seen in the 350 mA beam, by its loss when bunched, as well as the measured emittance value, is an effect of the higher current density.

Another possibly confusing factor in this region is the relatively high gas pressure ($\sim 10^{-4}$ Torr) which contributes (via negative ions and electrons) different neutralizing effects for the continuous beam and the bunched beam cases.

Beam Properties

What follows in this section is an experimental description of the particle motion in the 50 MeV machine at accelerated currents of 50 - 100 mA, with

emphasis on the transverse properties. As a background, we shall start with a resumé of the behaviour at 50 - 60 mA, quoting some results from a CERN Internal Report by Taylor and Tétu (Ref. 5).

Behaviour at 50 - 60 mA

- a) Expressing measured transverse characteristics in the form of density distributions, we found that gross mis-adjustments of RF levels and phases affected only the ends of the curves or the outer regions of the phase space at 50 MeV (Fig. 2).
- b) A comparison of density curves measured at 10, 30 and 50 MeV showed similarly differences only at the ends of the curves (Fig. 3).
- c) Comparison of 500 keV and 50 MeV density curves revealed a "blow-up" in total emittance by a factor of 3 (Fig. 4).
- d) A sieve, which reduces the amount of charge in the beam without appreciably changing the emittance, was placed across the 500 keV beam, and it was seen that the blow-up was independent of current at these current levels (Fig. 5).
- e) Successive collimation of the input beam by rectangular limitations in the phase plane, scaled to the original axis ratios, showed that removing phase space and current from the outside the phase space at 500 keV reduced the density over the whole phase plane at 50 MeV. (Fig. 6).

Summarizing, it seemed that the output density was determined essentially at energies below 10 MeV, that subsequent acceleration affected only the particles with maximum radial excursions (and maximum sensitivity to RF conditions), that there was blow-up which was independent of current up to 60 mA, and that particles anywhere in the input phase plane could be useful at the centre of the output phase plane.

The latter result and the fact that the charge distribution across the output phase planes is bell-shaped led one to suspect that a statistical approach might be profitable. Noting that the density curve is an invariant for linear transformations of ellipse shape at a given energy, we took a circular phase space envelope at the input and then applied to current elements in this plane a normal distribution defined by a standard deviation σ radially from the input co-ordinates (Ref. 6). The trapping loss was represented by a probability function P , the probability that a particle at the input should reach the output.

Fig. 7 shows the measured output density curve and the computed best fit curve for which $\sigma = 0.45$ of the input maximum radius and $P = 57\%$, both values

being constant over the phase plane. The agreement is close enough for one to say that our blow-up can be simulated by a simple model of normal scattering in the phase plane.

A physical interpretation is that couplings and non-linearities distort the 6-dimensional hypervolume statistically to yield a "blown-up" projection.

Following the set of measurements a) - e) above, an attempt was made to investigate some possible causes of blow-up.

Phase Coupling. One expects the radial effects of phase motion to be most pronounced in the regions of maximum phase and energy oscillation amplitudes at the beginning of the accelerator. The effect on the transverse density at the output should depend, therefore, on the distribution of particles across the energy-phase plane at the input. We have tried to demonstrate the importance of this effect experimentally by adjusting the buncher voltage and phase away from the nominal settings while maintaining the original value of 50 MeV current. What we found was that one setting of phase and voltage reduced the output emittance by 10% and increased the central phase space density at 50 MeV by 30% (Fig. 8). The effect is thus sufficiently pronounced to make it advisable to adjust buncher conditions on output density rather than on total current.

Quadrupole Couplings. Analytical and numerical work on quadrupole imperfections carried out by Regenstreif and Tanguy and reported at this Conference (University of Rennes in collaboration with CERN), has underlined the importance of the end-fields of short lenses on the coupling between horizontal and vertical motions.

Experimentally, work on single lenses which we are planning should be easier to interpret than measurements on the complete machine, but for the moment the latter are all we have. Firstly, at 500 keV, we have carried out a measurement of density in one plane for two different positions of a phase plane window in the other plane (Fig. 9). We next repeated the measurement at 50 MeV (Fig. 10) and we see that the difference is appreciable. Previously, we have interpreted this difference in vertical-horizontal dependence at 50 MeV and 500 keV as evidence of additional vertical-horizontal dependence introduced by the accelerator, either directly through the quadrupoles or indirectly through some other factor such as phase.

However, there is an alternative explanation for this tendency of particles to be grouped around both centres more at 50 MeV than at 500 keV. In simple terms, a particle which is near the centre in both planes will have a better chance of surviving aperture limitation than a particle which is away from the centre in one or both planes. Particle loss will, in other words, be selective, leading to the behaviour of Fig. 10.

Summarizing the measurements on coupling, we find some evidence that phase coupling (below 10 MeV) plays a rôle in determining the final transverse density, but the evidence from the Linac for vertical-horizontal coupling is inconclusive.

We conclude with two remarks concerning the form of the 4-dimensional hypervolume, which is often taken to be a 4-dimensional hyper-ellipsoid. The first point is that emittance envelopes are only approximately ellipses, and contours only approximately concentric (see Fig. 15). The second point is that hyper-ellipsoid geometry predicts certain effects (pointed out to us by Regenstreif and Tanguy) which we do not observe. The geometry precludes that particles on the envelope at one plane be simultaneously on the envelope of the other, and in fact permits that they be only at the centre. This implies that aperture limitation at the outside of one plane should reduce the density only near the centre of the other, whereas we find always a general reduction over the whole plane.

Behaviour at 100 mA

As may be expected from our earlier remarks on trapping efficiency, the gain in 50 MeV density by no means followed the gain in 500 keV density when the new pre-injector was installed, although the general pattern of blow-up remained the same (Fig. 11).

The most important difference so far revealed has been in the effect of acceleration above 10 MeV. The first measurements of 10, 30 and 50 MeV densities at 100 mA showed that the densities deteriorated with energy over the central regions instead of just at the edges. It was then observed that the 50 MeV density was more sensitive to the phase of Tank II with respect to I and III than previously. At the first opportunity, therefore, tank phases were added to the parameters hitherto used for "optimizing" the machine. Adjusting now the input energy, buncher phase and voltage, tank phases and levels, and radial matching and focusing, the machine was trimmed to give maximum current through a 4-dimensional radial limitation at 50 MeV. The result was that the differences between the 10 and 50 MeV densities were appreciably closed as may be seen in Fig. 12. (The reason for the change in 10 MeV density is not known. There was a week between the sets of measurements.)

As yet there has not been sufficient time for much investigation of this matter. It seems likely though that at 100 mA there is a greater proportion of the particles out towards the stability limits in the longitudinal plane than at 50 - 60 mA, because of space charge and inefficient trapping, causing particle loss to become more sensitive to RF conditions.

One sees here the need for measurements in the longitudinal plane along the accelerator.

Beam Effects

Beam Loading

Since last November, the machine has been operated with a mixed system of beam loading compensation. That is, Tanks I and II receive additional power during the beam by means of mismatches in the modulator delay lines, while Tank III is fed by two final amplifiers and loops, one for the main excitation, with 200 μ s pulse, and the other for the beam power, with a pulse lasting for approximately the duration of the beam pulse, 20 μ s. With this temporary arrangement and with the use of the debuncher it has been possible to keep the total energy spread within reasonable limits, around \pm 200 keV at 100 mA.

A complete compensating chain of power amplifiers has now been installed and in the coming months the system will be commissioned. Fig. 13 shows the final arrangement.

With the Tank III separate feed, we have been able to test to reduce the $\frac{dV}{dt}$ in the tank to a very low value during the pulse, producing under-compensation, compensation or over-compensation at will by means of the compensation modulator control.

The setting-up of the two feeds proves to be fairly straight-forward in practice. The compensation amplifier is tuned for maximum power and then the feeder length is adjusted to minimize the power transfer backwards to the compensation amplifier which is passive during the tank build-up and presumably offers a diode impedance. In fact, since the anode tuning acts on the electrical length from the tank loop to the triode, the anode tuning can also be used to minimize the power transfer backwards provided that one is not too far from the maximum power output setting.

The compensating amplifier drive contains a phase shifter as is seen from Fig. 13, and this can be used to adjust for the "in-phase" condition from the tank level, and subsequently the ϕ s condition.

The present compensating loops are of the same dimensions as the excitation loops, but as the compensation feeder sees a lower impedance at the tank terminals, that is, the shunt impedance in parallel with the beam-power impedance, it may be worthwhile modifying the compensation loops to match this lower impedance to the amplifier.

As an intermediate step, the 20 μ s compensating pulses are obtained from delay lines, but in the future we hope to derive pulses variable up to 50 μ s in length by control of the grid bias of the power amplifiers. On test, we have already controlled

output powers from zero to 1.5 MW by controlling the bias.

Beam Damage

It has already been mentioned under Bunching that the beam has left traces of melting on stainless steel. Fig. 14 shows the damage caused to a set of thin Al plates used in the 4-jaw apertures at the entry of Tank I. This damage announced itself by a rise in current downstream from the apertures during an experiment.

At this point, the beam power is of the order of 250 kW for 20 μ s, i.e. 5 Joules are released by total absorption.

When these apertures were repaired, the opportunity was taken to inspect the drift tubes in Tank I. Fortunately, there were no new signs of damage after three months' running.

RF Breakdown

Practically the first effect of the new pre-injector beam was that RF breakdown occurred in Tank I. It was soon found, however, that correct steering and focusing could eliminate this.

Since the range of 500 kV protons in copper is very short, it is possible that any metallic or non-metallic surface irregularity in the way of the beam would be heated to a high temperature and would produce vapour and electrons, leading eventually to a discharge across the gap.

Instrumentation

Automatic Emittance Measurements

An automatic emittance measurement and analysis system has been developed for use in the many Linac experiments involving emittance determinations. The aims were:

- a) to speed up the measurements;
- b) to enable more lengthy or complex experiments to be performed, for example emittance measurements at several positions (simultaneously in the beam pulse);
- c) to provide complete and objective analysis of the results;
- d) to give immediate results via an on-line computer.

Only d) remains unfulfilled and this awaits the installation of the CPS control computer.

Consider briefly the manual method used for emittance measurement (Ref. 7). After the Linac, a slit 2 mm wide defines a strip of the output proton beam in phase space at a constant vertical or horizon-

tal position. This slice of beam passes through a focusing triplet, at the focal plane of which, and parallel to the first slit, is another 2 mm wide slit defining a small range of angular divergence. The current passing through the two slits is measured with a transformer and by moving the slits systematically and recording the current at each elemental area (2 mm x 0.584 mrad), the emittance plane can be mapped.

When the automatic system is used four parameters are recorded for each point in the phase plane, the position, angle and elemental current, with the total Linac output current as a normalizing and checking parameter. Initially, preset range limits are set up on the slit control boxes. Then starting from one corner of the defined phase plane, the current passing through the two slits is measured (and accepted as valid when the total current is above a preset level) before moving the angle defining slit to define the adjacent emittance element. The recording system used (Ref. 8) converts the four analogue signals to numbers on a linear scale of 0 to 255 and punches the coded results on five hole paper tape. After the paper tape data have been transferred to magnetic tape, the analysis is done on the CDC 6600 computer. When the on-line computer becomes available, the analogue signals can be processed directly. The raw data of elemental currents can be represented by a 3-dimensional histogram with the emittance plane as the base. By fitting a smooth analytical surface to these data parallelepipeds, emittance areas and integrated currents contained within equicurrent lines are readily derived. Suppose the position and angle co-ordinates are u , v , then treating each elemental emittance area as a square (geometrically), we can fit a function for the current variation.

$$J(u,v) = [a_1u^2 + b_1u + c_1]v^2 + [a_2u^2 + b_2u + c_2]v + a_3u^3 + b_3u + c_3$$

This form, though appearing complex, allows the variation of current within an elemental square to be influenced by the currents in the eight nearest elemental squares. The fitting criteria are

- a) the current integrated over the elemental square equals the measured current;
- b) the values of currents (but not necessarily the slopes) are continuous across the boundaries between neighbouring squares);
- c) the nine fitted values will be exact when the actual coefficients are constant over the whole plane.

Using the derived coefficients, each unit square is examined to see if any equicurrent lines prescribed in the input data pass across it. If this is so, then the current and emittance inside the equicurrent contour are calculated and symbols are set in the computer line-printer format giving the approximate position of the equicurrent line. A typical output is shown in Fig. 15. (The discon-

tinuous nature of contour A is not significant). The equicurrent lines define the maximum currents within the corresponding emittances so that the calculated results give unambiguous points on a current versus emittance curve. With stable Linac conditions this automatic system gives good reproducible results, especially for the numerical values.

Statistical Analysis

By use of a prototype version of the present data logging system (Ref. 8) some results on stability of Linac parameters were obtained and presented previously (Ref. 5). Since then, there has been considerable development of the analysing computer programs (Ref. 9) and some consideration of the statistical analyses which might be made with an on-line computer. The more common descriptive statistical techniques such as the graphical representations of frequency distributions and moving averages of parameters presented no particular programming problems. For inductive statistical analyses, the programming of the data reduction is more difficult but the real problems lie in the design of suitable experiments which can give significant results for the testing of hypotheses.

It was hoped to be able to isolate important parameters by measuring their correlations with other key operating parameters of the CPS, e.g. the circulating beam intensity and mains voltage. Some significant correlations were found but these changed (sometimes in algebraic sign) from experiment to experiment. One concludes that many unmeasured factors affect the actual multiple correlations found and that it may be more profitable to use other less rigorous but more flexible and empirical methods of analysis.

A linear regression program was developed to give the best statistical fit of, for example, measured values of output current to a function of several optimizing variables. The functional forms found would be useful in the choice of a strategy for automatic optimization.

Conclusions

There seems to be one essential difference between the behaviour of the 50 MeV machine at 50 mA and at 100 mA. At 50 mA one can still treat the transverse properties and longitudinal properties separately as a working approximation and adjust RF conditions for the best energy spread, leaving transverse properties very largely to the ion source, focusing fields and the various perturbations and couplings along the machine. However, at 100 mA there seems to be less room around the bunch in the RF bucket, and the smooth progression of the bunch along the machine is of direct importance to the particle loss and therefore to the transverse density.

We consider that improvements in the transverse density in the future will come most easily from improvements in the bunching process.

Acknowledgements

We gratefully acknowledge our indebtedness to all of our colleagues in the Linac Group, in particular to B. Vošicki and J. Huguenin, who made higher currents possible. We thank also H.G. Hereward and P. Lapostolle for useful discussions.

APPENDIX I

3 MeV Model

Within the framework of the MPS Improvement Programme, we have started the design of a short section of Alvarez structure, from injection energy up to about 3 MeV. This model will be installed on the beam line of the existing experimental pre-injector and this arrangement will permit us to investigate experimentally the particle dynamics of the bunching and trapping processes. Eventually, on the basis of this work, we hope to be able to fix the parameters of a new Tank I for the 50 MeV Linac.

APPENDIX II

CPS RF Ion Source Work (Ref. 10)

Before the installation of the duoplasmatron source, a series of emittance measurements was made using a scanning Faraday cup on the old accelerating column with the RF ion source. The measurements were later repeated in the laboratory, just behind the source outlet. Our results (Table I) show a considerable blow-up of the emittance by a factor of 6 - 12 times between source and column end. The shape of the source emittance changes from a fairly straight line at low beam current levels (45 mA) to an S-shape at higher currents (see Figs. 16 and 17). At the column end, 45 mA gives a reasonable shape (Fig. 16), going into a more complex pattern at higher currents (Fig. 18). Iso-density contours had earlier been recorded with the scanning Faraday cup, giving an interesting quadrupolar symmetry when the first triplet lens was working (Fig. 19). To simplify the interpretation of the above-mentioned emittance measurements, these were done without the first triplet lens working.

Some time ago, a re-design of the RF source was undertaken with a view to incorporating it in a short column (Fig. 20). The source works stably at beam currents of 750 mA (86 bad pulses on 10 000 good ones) with a 20 microsecond pulse of 22 kV on the anode, and 15 kV pulse on the Pierce electrode. At higher extraction levels, currents above 1 ampere have been observed but breakdowns then become rather frequent (Fig. 21).

References

1. B. Vošicki, M. Buzić and A. Cheretakis, "The Duoplasmatron Source for the CERN-PS Linac", Oct. 1966, this Conference, p. 344.
2. J. Huguenin, R. Dubois, G. Visconti and R. El-Bez, "The New 500 keV Single-gap Pre-injector Tube for the CERN-PS Linac", Oct. 1966, this Conference, p. 355.
3. B.I. Bondarev and A.D. Vlasov, "Self-consistent Particle Distribution and the Current Limit in Linear Accelerators", Proceedings at the 5th International Conference on High Energy Accelerators, Frascati 1965.
4. M. Chororow and L.T. Zitelli, "The Radio-frequency Current Distribution in Brillouin Flow", I.R.E. Transactions on Electron Devices 1959, Vol. 7, p. 352.
5. C.S. Taylor and P. Têtu, "Transverse Properties of the PS-Linac Beam" March 1966, CERN Internal Report, MPS/Int.LIN 66-2.
6. R. Keyser, CERN DD Division, Private communication.
7. C.S. Taylor, "High Current Performance of the CERN-PS Linac", International Conference on High Energy Accelerators, Dubna 1963
8. U. Kracht, "Data Logging Used on a Proton Linear Accelerator and a Description of the Analogue to Digital Converter Used", Nuclear Instruments and Methods, Vol. 37, p. 231, 1965.
9. D.J. Warner, "Computer Analysis of Data Obtained with the CPS Linac Data Logging System" and U. Kracht, "Appendix on the Present State of the Data Logging System", CERN Internal Report, MPS/Int.LIN 66-6, Sept. 1966.
10. U. Tallgren, "Progress Report on the CPS RF Ion Source Work", CERN Internal Report, MPS/Int. LIN 66-8.

DISCUSSION

C. TAYLOR, CERN

EMIGH, LASL: In your emittance measuring device, did you use swept fields or a number of Faraday cups; or what was the detail?

TAYLOR: We use slits and a lens to define a small element in the phase plane, followed by a beam transformer to measure the current within the element.

MILLER, SLAC: Are your emittances therefore the projection from the four-dimensional (x, y, P_x, P_y) space on to two-dimensional (x, P_x) space?

TAYLOR: From the six-dimensional space.

FEATHERSTONE, Univ. of Minnesota: You didn't mention the possibility that some of the difference in performance between the radiofrequency source and the duoplasmatron might be related to the different proportions of protons produced by them.

TAYLOR: The rf source delivered between 85 and 90% of protons, and the figure for the duoplasmatron is also about 85%.

HUBBARD, LRL: You mentioned having beam compensation on the first and third tanks. What's the situation of the second one?

TAYLOR: The complete compensating chain is now installed -- that is, feeders, loops, power amplifiers, and cables -- and it's just a matter of time.

HUBBARD: Your present measurements do not include any compensation there?

TAYLOR: I'm sorry. I should have mentioned that the emittance measurement is gated over a micro-second or so at any point within the pulse, and this eliminates the first-order effect of beam loading.

HUBBARD: It eliminates the time dependence then?

TAYLOR: Yes.

GIORDANO, BNL: Were any measurements made of relative phase and amplitude between the ends of a single tank as a function of beam loading?

TAYLOR: Not recently with the higher currents.

VOGEL, ANL: I heard you mentioning that you had reached the space charge limitation. Just where in the machine would this be?

TAYLOR: A priori, in the bunching or in the early gaps of the machine; but we don't know which yet. We think it's best to look at the bunching first. I believe that someone in this conference is going to direct our attention towards the end of the machine.

CURTIS, MURA: Out of the preinjector for a given fraction of the current in the phase ellipse, how has the emittance increased with increasing current?

VOSICKI, CERN: The source can be adjusted to give currents of between 300 and 700 mA within substantially the same emittance.

CURTIS: What is the value of this emittance?

VOSICKI: A typical value for 650-700 mA is about 0.7 cm-mrad normalized.

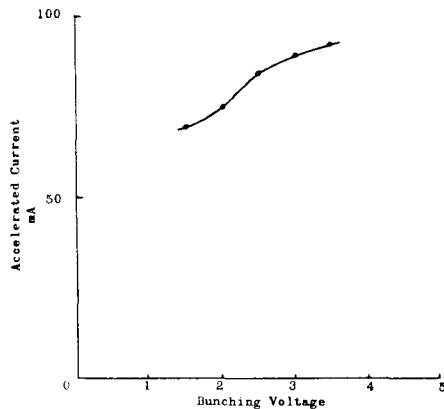


Fig. 1. Dependence of accelerated current on bunching voltage.

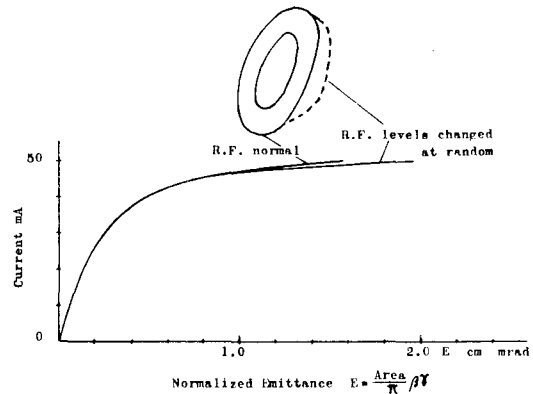


Fig. 2. Effect of RF levels on 50 MeV density curve.

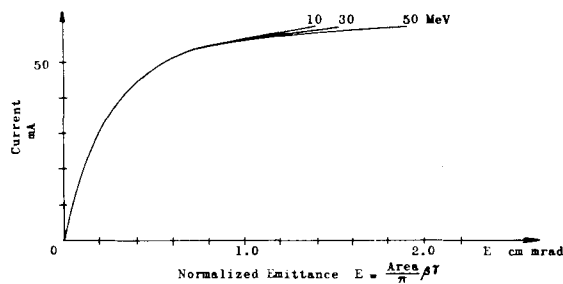


Fig. 3. Density curves for 10, 30, and 50 MeV.

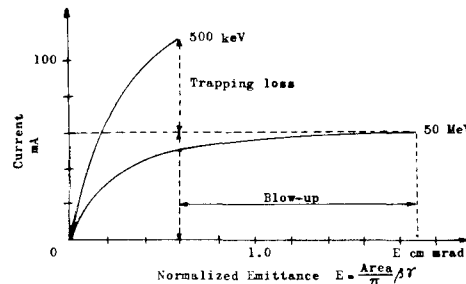


Fig. 4. Comparison of 500 keV and 50 MeV density curve.

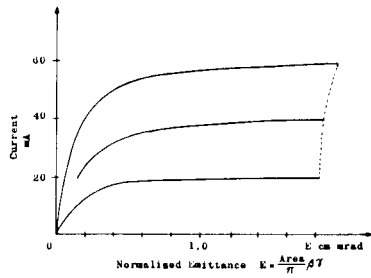


Fig. 5. 50 MeV density curves when 500 keV beam is reduced in current but not in emittance.

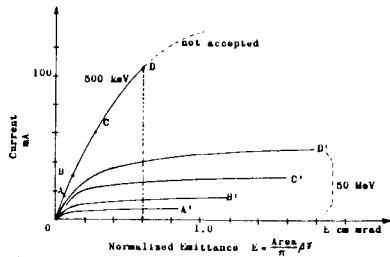


Fig. 6. 50 MeV density curves for collimated 500 keV beam.

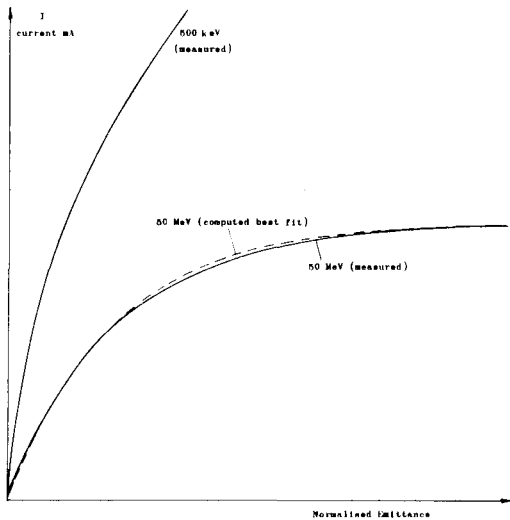


Fig. 7. Blow-up computed from measured 500 keV beam by distributing particles normally in the phase plane. Compared with 50 MeV measurement.

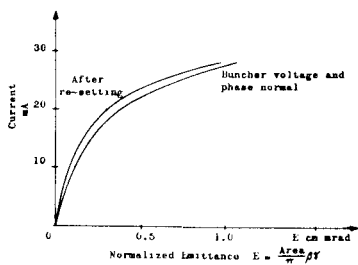


Fig. 8. 50 MeV density curves for two different bunching conditions.

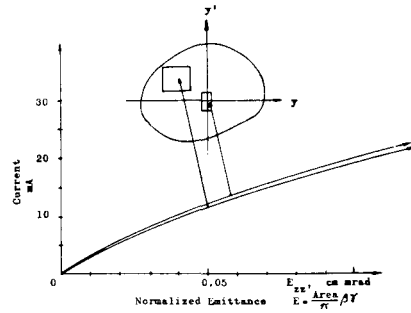


Fig. 9. 500 keV density distributions in zz' plane of equal currents selected from different regions of yy' .

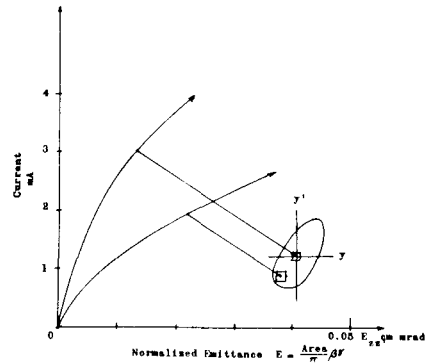


Fig. 10. 50 MeV central density distributions in zz' plane of equal currents selected from different regions of yy' .

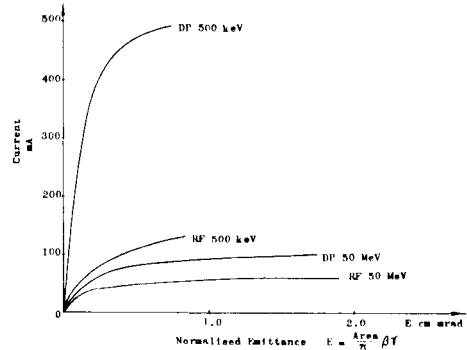


Fig. 11. Comparison of density curves at 500 keV with 50 MeV for RF source and duoplasmatron.

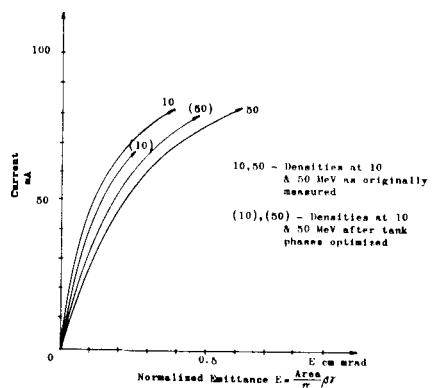


Fig. 12. Effect of tank phases on 50 MeV density.

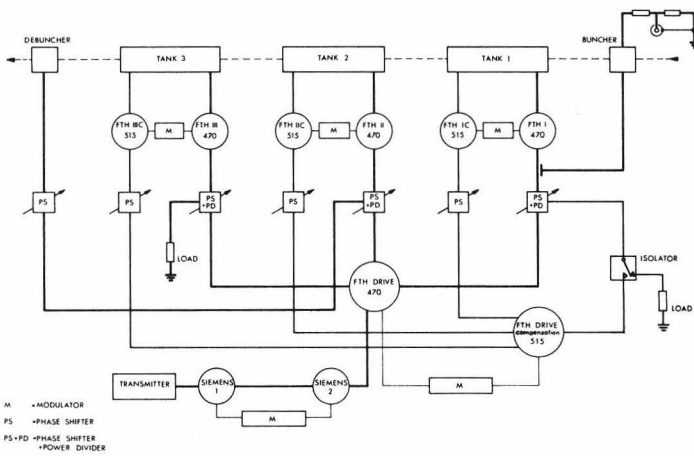


Fig. 13. RF system with beam loading compensation chain.

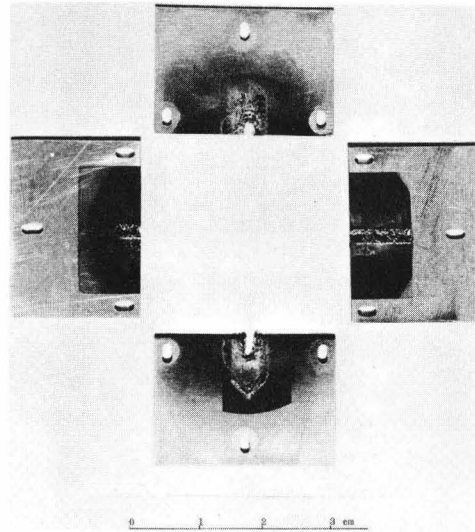


Fig. 14. Beam damage to 500 keV apertures.

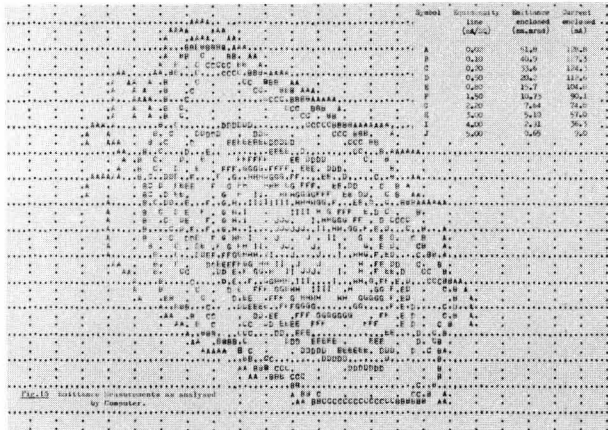


TABLE I
RF Source

Source Extraction Voltage	Beam Current	Emittance measured at the source		540 keV Emittance measured at the column end	
		mm mrad	$\frac{\text{Area}}{\pi} \beta\gamma$ cm mrad	mm mrad	$\frac{\text{Area}}{\pi} \beta\gamma$ cm mrad
10	45	21	$9.7 \cdot 10^{-3}$	35	$12 \cdot 10^{-2}$
15	90	38	$21 \cdot 10^{-3}$	44	$15 \cdot 10^{-2}$
20	150	69	$45 \cdot 10^{-3}$	115	$39 \cdot 10^{-2}$
27	230	102	$78 \cdot 10^{-3}$		
27	190			110	$39 \cdot 10^{-2}$

Fig. 15. Emittance measurements as analyzed by computer.

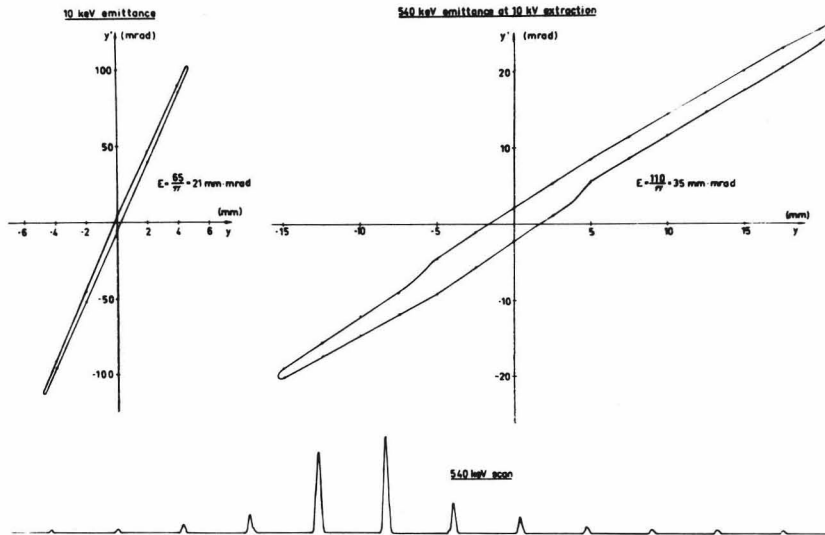


Fig. 16. RF source and pre-injector emittance at 45 mA beam current.

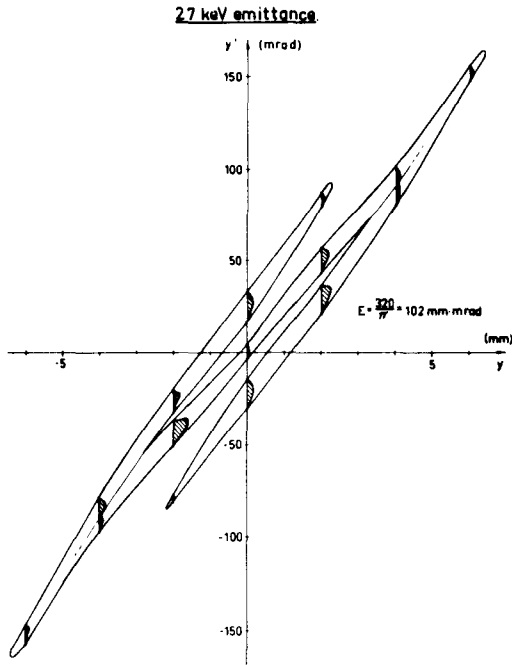


Fig. 17. RF source emittance at 230 mA beam current.

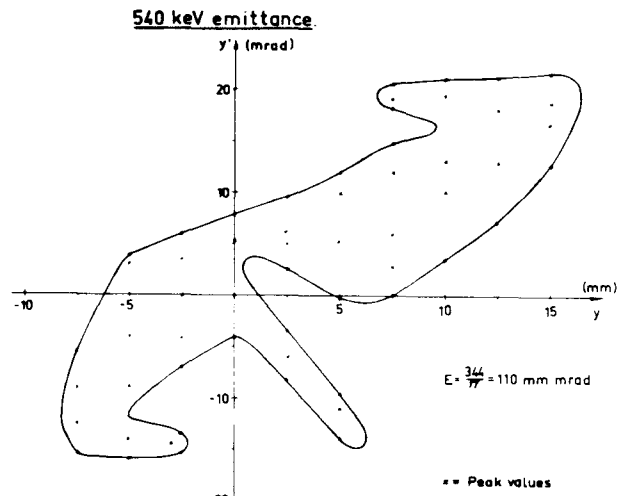


Fig. 18. Pre-injector emittance at 190 mA beam current with RF source.

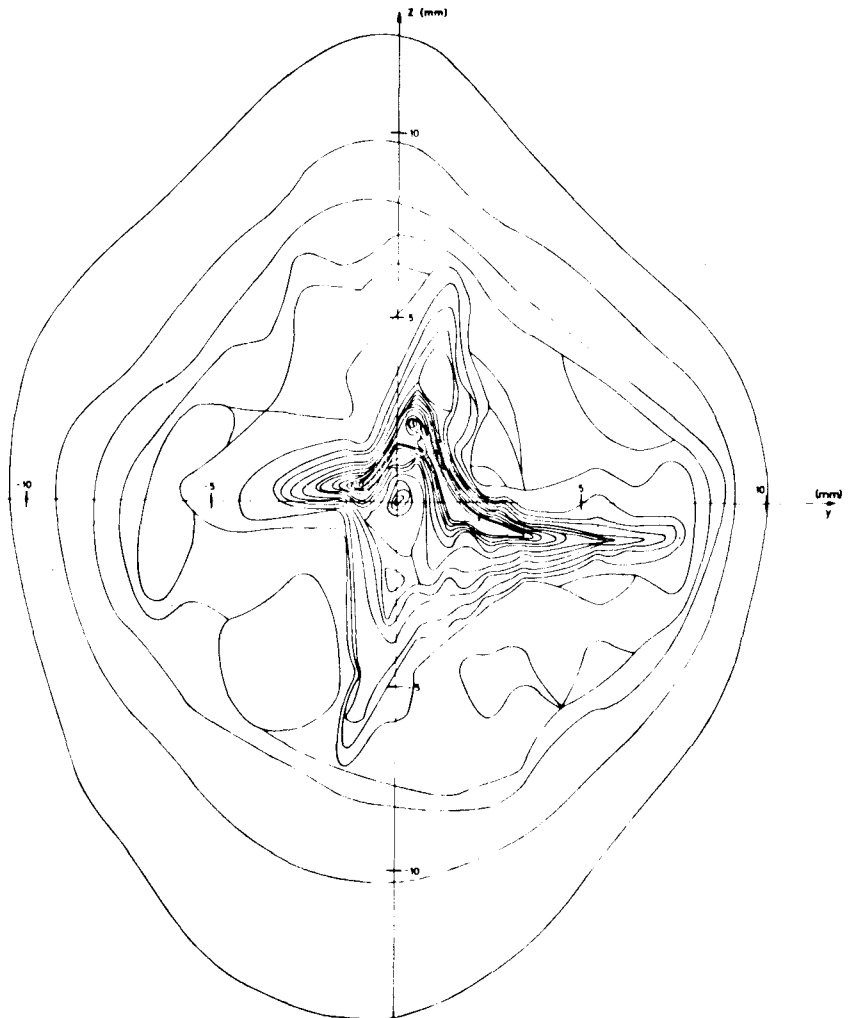


Fig. 19. Iso-density contours of pre-injector beam focused by the triplet lens (RF source).

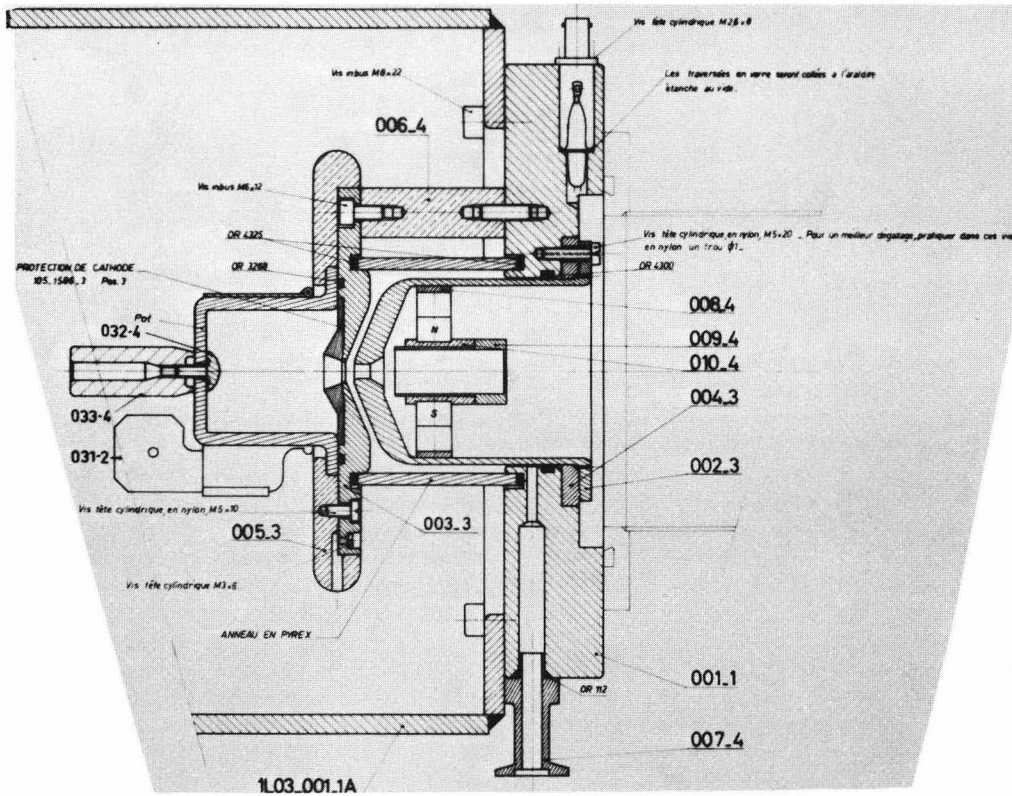


Fig. 20. Lay-out of experimental RF ion source.

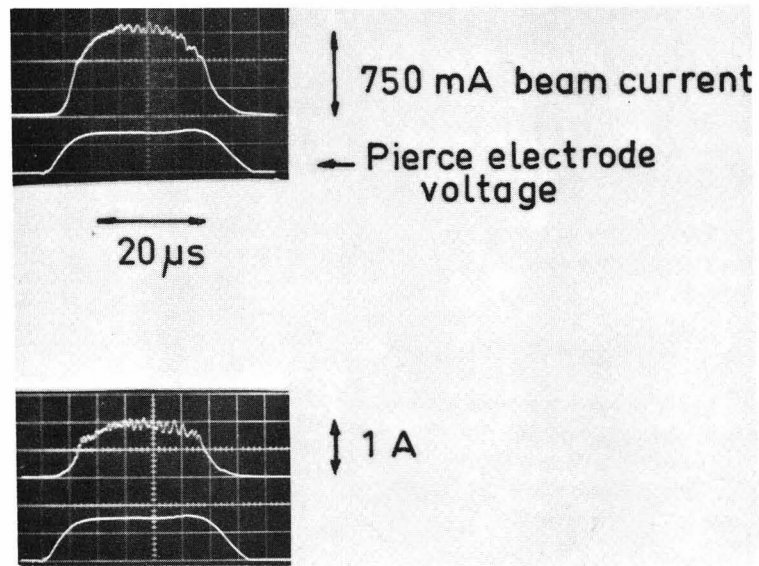


Fig. 21. Oscilloscope pictures of beam current from experimental RF ion source.